Catalytic Role of Vacancy Diffusion in Ceria Supported Gold Catalyst

Zhong-Kang Han, Yang-Gang Wang* and Yi Gao*

Methodology:

The spin-polarized density functional theory (DFT) with the PBE (Perdew-Burke-Ernzerhof) functional[S1] as implemented in the Vienna ab initio simulation package (VASP) was employed.[S2,S3] A Hubbard-U term using the Dudarev approach[S4] was added to the PBE functional (DFT+U) to account for exchange and correlation. The value of U=5.0 eV as suggested initially by Nolan *et al.* was used to obtain localized electron distribution.[S5] Previous studies indicated that multiple self-consistent solutions exit, corresponding to different occupations of the *m* projections associated with the *f*-shell to which the U parameter is applied.[S6,S7] These solutions may differ in total energy by up to 0.3-0.4 eV for CeO_2 bulk or surface containing an oxygen vacancy. However, in this work, the used Davidson-block iteration scheme with random initialization of the orbitals, for which most extensive tests have been performed, is considerably robust.[S8] The valence electronic states were expanded in the basis of plane waves, with the core-valence interaction represented using the projector augmented wave (PAW) approach[S9] and a cutoff of 400 eV. Different U values and energy cutoff are also applied to examine the reliability of our results. It is found that they quantitatively affect the relative energies very slightly (Table S3). We treated the Ce (4*f*, 5*s*, 5*p*, 5*d*, 6*s*) and O (2*s*, 2*p*) electrons as valence states, whereas the remaining electrons were kept frozen as core states in the PAW method. The CeO_2(111) (4×4) and (4×6)) slabs with nine atomic layers were used to simulate the ceria support for single gold adsorption and gold dimer adsorption, respectively. The bottom 3 atomic layers were fixed to mimic bulk structure, during the relaxation. The Γ point sampling was employed for Brillouin Zone integration. A larger (6*6) supercell and a larger k points sampling (2×2×1) were also considered to test the convergence (Table S2). The transition-state (TS) structures were located by the climbing image nudged elastic band (CI-NEB) method[S10] to identify the minimum energy paths on the potential energy surface, with the maximum force converged to 0.02 eV/Å. These calculations have been performed in the above mentioned supercells including at least 5 replica images between the initial and the final geometries.

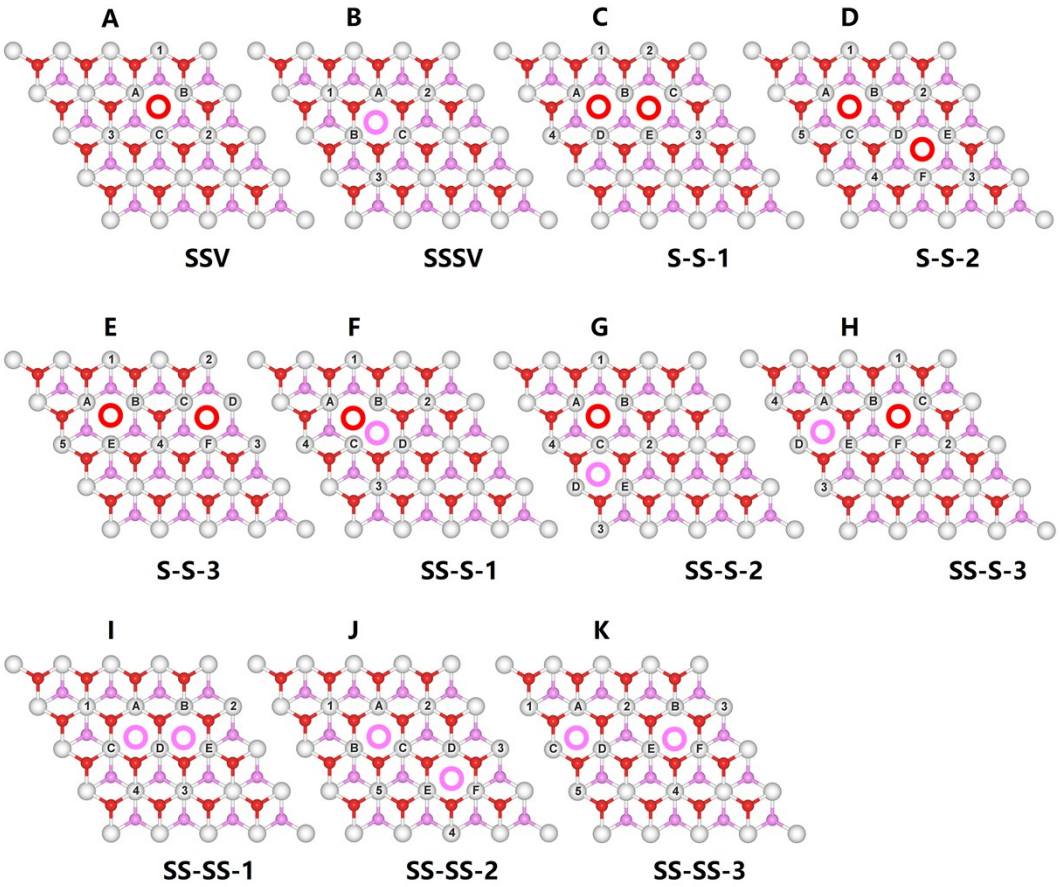

Figure S1. Structural models of different types of near-surface oxygen vacancy on reduced CeO_2(111). In S(SS)-S(SS)-N, S(SS) means surface O_v (subsurface O_v) and N means they are in the nth nearest neighbor site. Cerium, surface oxygen, and subsurface oxygen atoms are depicted in white, red, and pink, respectively. Open circles represent oxygen vacancies. For clarity, only the first O–Ce–O trilayer (TL) is shown. The labelled cerium atoms denote possible Ce^{3+} locations on nearest-neighbor (A, B, C, D….) or next-nearest-neighbor (1, 2, 3, 4….) sites to the vacancies.

Table S1. Oxygen vacancy formation energy for different types of near-surface oxygen vacancy on reduced CeO_2(111). $\Delta^{E_v^a}$ is the average formation energy per oxygen vacancy. Calculated with p (4×6) periodicity, 3 CeO_2 trilayers and Γ-point. The configurations of the 4*f* electrons are corresponding to Figure S1.

Types	Configurations $\Delta^{E_v^a}$ (eV)						
SSV	23 2.10	2-A 2.12	AB 2.29				
SSSV	13 1.91	1-B 2.09	AC 2.21				
S-S-1	12-DE 2.16	34-BE 2.17	24-BE 2.18	124-E 2.19	134-B 2.20	4-BCE 2.22	BCDE 2.26

	1-BCD 2.27	1234 2.28	14-BE 2.28				
S-S-2	245-D 2.11	124-D 2.11	24-AD 2.11	1235 2.12	2345 2.12	123-D 2.13	45-BD 2.14
	12-DF 2.14	2-BDF 2.17	234-A 2.18	15-EF 2.18	5-BDF 2.19	4-ADE 2.19	235-A 2.19
	25-AF 2.19	345-B 2.23	35-BF 2.25	BCDF 2.27			
S-S-3	1245 2.15	345-B 2.16	1345 2.16	145-D 2.18	45-BD 2.18	245-B 2.19	135-C 2.22
	124-A 2.23	14-AD 2.24	35-BC 2.24	25-BF 2.24	125-F 2.26	1235 2.27	12-EF 2.29
	1-CDE 2.29	4-ACD 2.30	15-BF 2.31	5-CDF 2.34	ABDF 2.36		
SS-S-1	123-B 2.23	24-BC 2.34	14-BC 2.40	34-BC 2.40	1-BCD 2.41	12-BC 2.45	ABCD 2.49
SS-S-2	1234 2.16	134-C 2.18	234-C 2.20	123-C 2.23	23-BC 2.24	12-CE 2.25	13-BC 2.28
	14-CD 2.30	1-CDE 2.33	2-BCE 2.34	24-BC 2.34	4-ACE 2.44	BCDE 2.47	
SS-S-3	24-BE 1.96	234-B 1.98	124-E 2.01	23-AB 2.02	13-CE 2.03	12-BE 2.03	14-EF 2.05
	134-F 2.05	1234 2.07	34-BE 2.10	1-DEF 2.12	4-BDF 2.12	2-BDF 2.13	BCEF 2.17
SS-SS-1	124-D 2.03	12-AD 2.05	13-BD 2.05	134-B 2.06	1234 2.08	34-AB 2.10	14-BD 2.12
	4-ABE 2.13						
SS-SS-2	134-C 1.90	2345 1.94	1245 1.95	123-E 1.98	1234 1.99	35-AC 1.99	13-CE 2.00
	34-BC 2.01	235-E 2.01	23-CE 2.03	234-E 2.04	125-F 2.07	12-EF 2.10	25-AF 2.11
	ACEF 2.14	2-BEF 2.15					
SS-SS-3	2345 1.89	1234 1.90	124-D 1.93	245-C 1.94	1345 1.96	123-D 1.98	125-F 2.00
	13-DE 2.02	135-E 2.04	145-B 2.04	14-BD 2.05	2-CEF 2.06	15-BE 2.08	45-BD 2.09
	1-DEF 2.13	5-AEF 2.14	2-CDF 2.16	CDEF 2.23			

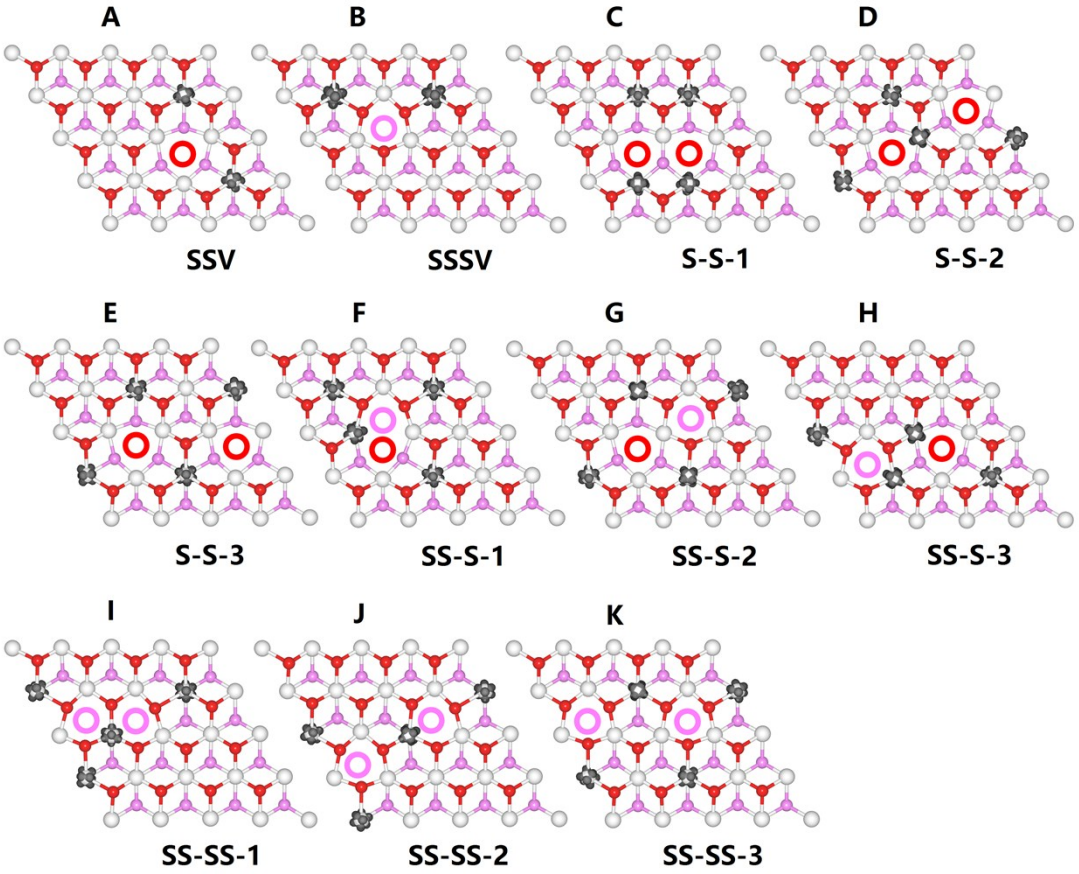

Figure S2. Structures of the lowest-energy configurations of different types of near-surface oxygen vacancy on reduced CeO_2(111). In S(SS)-S(SS)-N, S(SS) means surface O_v (subsurface O_v) and N means they are in the Nth nearest neighbor position. Cerium, surface oxygen, and subsurface oxygen atoms are depicted in white, red, and pink, respectively. Open circles represent oxygen vacancies. For clarity, only the first O–Ce–O trilayer (TL) is shown.

Table S2. Test calculations of a bigger supercell and k-points for the oxygen vacancy formation energy for different types of near-surface oxygen vacancy on reduced CeO_2(111). $\Delta^{E_v^a}$ is the average formation energy per oxygen vacancy.

Type	ΔE/eV			
	Γ point		2×2×1 *k* points	
	p(4*6)	*p*(6*6)	*p*(4*6)	*p*(6*6)
S-S-1	2.16	2.15	2.16	2.15
S-S-2	2.11	2.07	2.12	2.07
S-S-3	2.15	2.09	2.15	2.09
S-SS-1	2.23	2.29	2.23	2.30

S-SS-2	2.16	2.10	2.17	2.10
S-SS-3	1.96	1.99	1.96	1.99
SS-SS-1	2.03	2.01	2.03	2.01
SS-SS-2	1.90	1.95	1.91	1.90
SS-SS-3	1.89	1.86	1.89	1.86

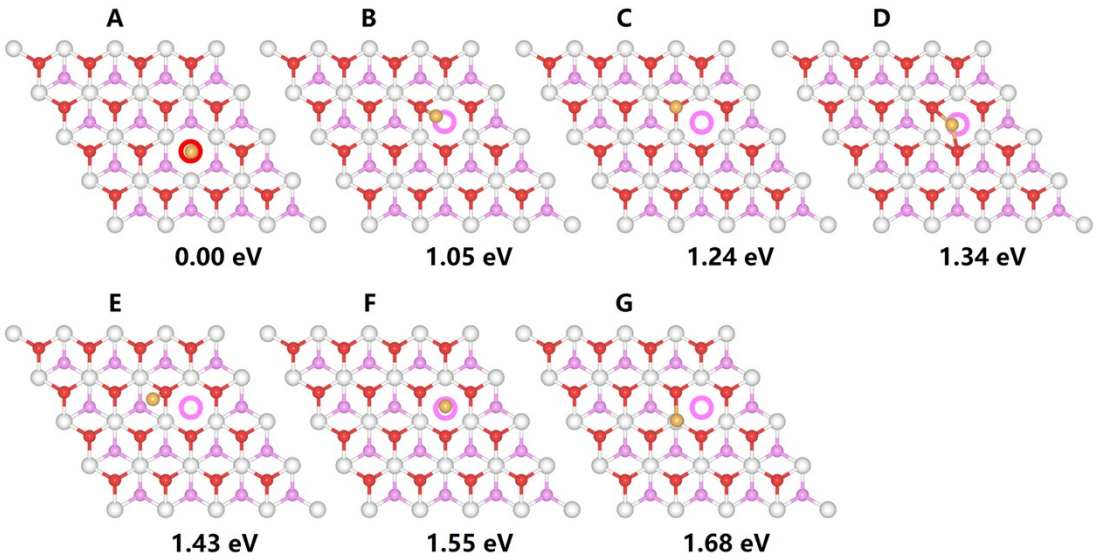

Figure S3. Structures of $Au_1@CeO_2(111)$ surface with SSV (A) and SSSV (B, C, D, E, F and G). Cerium, surface oxygen, and subsurface oxygen atoms are depicted in white, red, and pink, respectively. Open circles represent oxygen vacancies. For clarity, only the first O–Ce–O trilayer (TL) is shown. Energies are relative to the most stable structure.

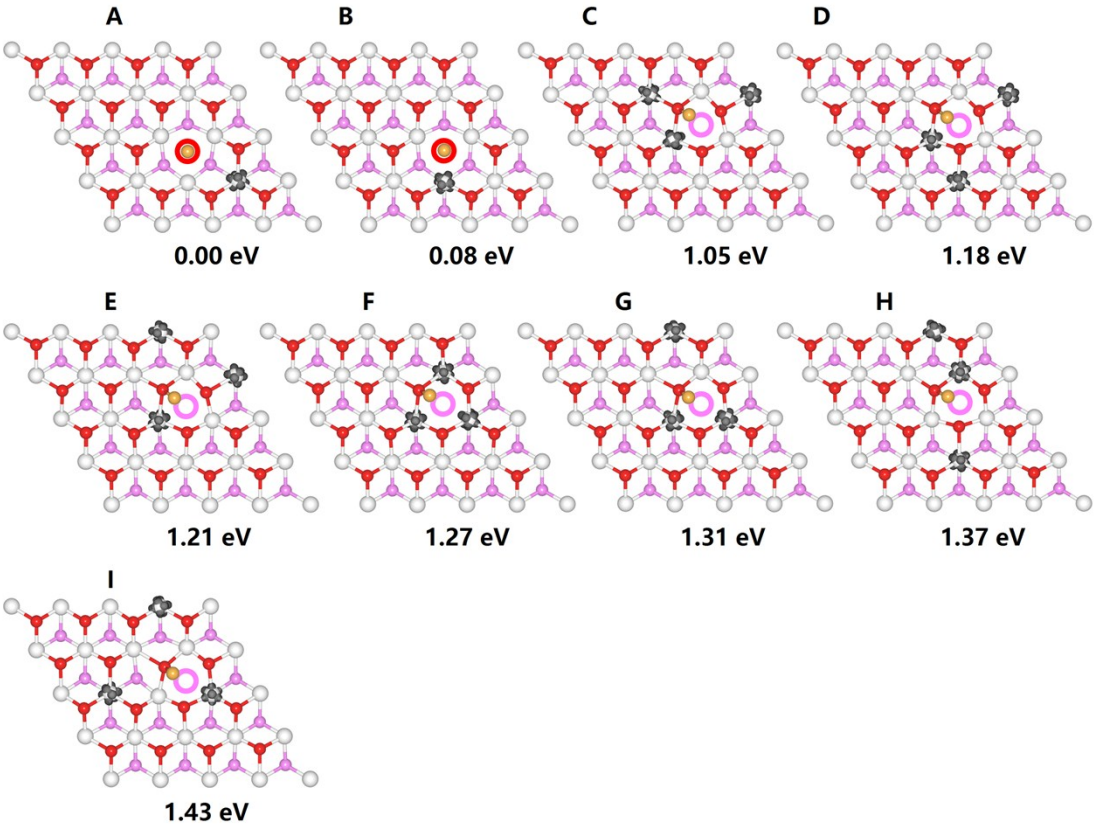

Figure S4. Multiple configurations of the excess 4*f* electrons on the most stable $Au_1/CeO_2(111)$ surface with SSV (A and B) and SSSV (C, D, E, F, G, H and I). The isosurface (0.02 e/Å) of calculated spin charge is in dark. Cerium, surface oxygen, and subsurface oxygen atoms are depicted in white, red, and pink, respectively. Open circles represent oxygen vacancies. For clarity, only the first O–Ce–O trilayer (TL) is shown. Energies are relative to the most stable structure.

Table S3. Test calculations of different U values (U = 4.5 eV and 5.0 eV), thicknesses (9L and 12 L), and energy cutoffs (400 eV and 500 eV) for the adsorption of gold monomer on reduced $CeO_2(111)$.

Type	ΔE (eV)/N (number of the unpaired electrons)					
	U = 4.5 eV			U = 5.0 eV		
	9L; 400 eV	9L; 500 eV	12L; 500 eV	9L; 400 eV	9L; 500 eV	12L; 500 eV
Au_1@SSV	2.31/1	2.32/1	2.32/1	2.24/1	2.24/1	2.25/1
Au_1@SSSV	1.25/3	1.25/3	1.26/3	1.19/3	1.19/3	1.20/3

$Au_2@CeO_2(111)$-S-S-1

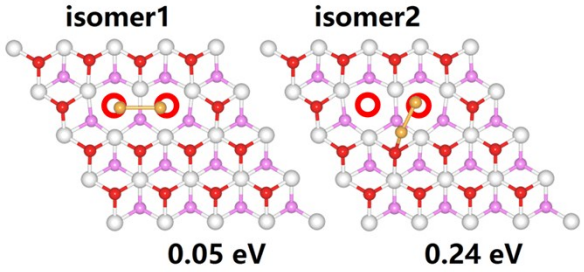

$Au_2@CeO_2(111)$-S-S-2

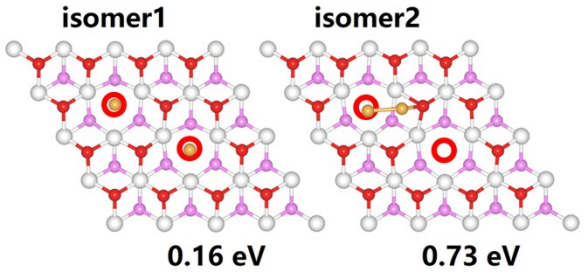

$Au_2@CeO_2(111)$-S-S-3

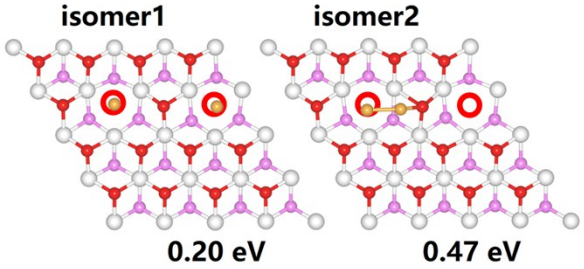

$Au_2@CeO_2(111)$-SS-S-1

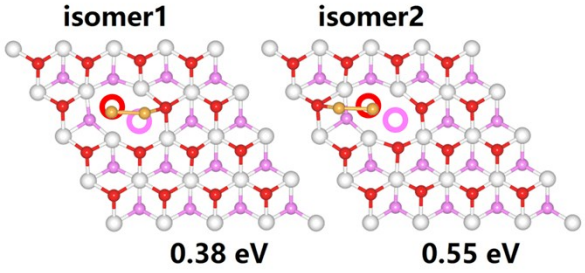

$Au_2@CeO_2(111)$-SS-S-2

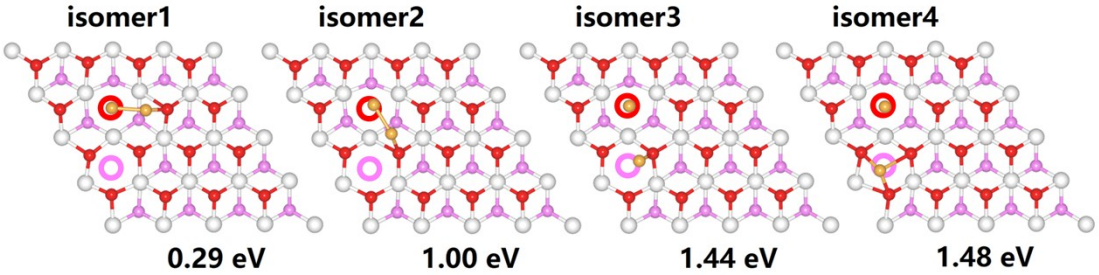

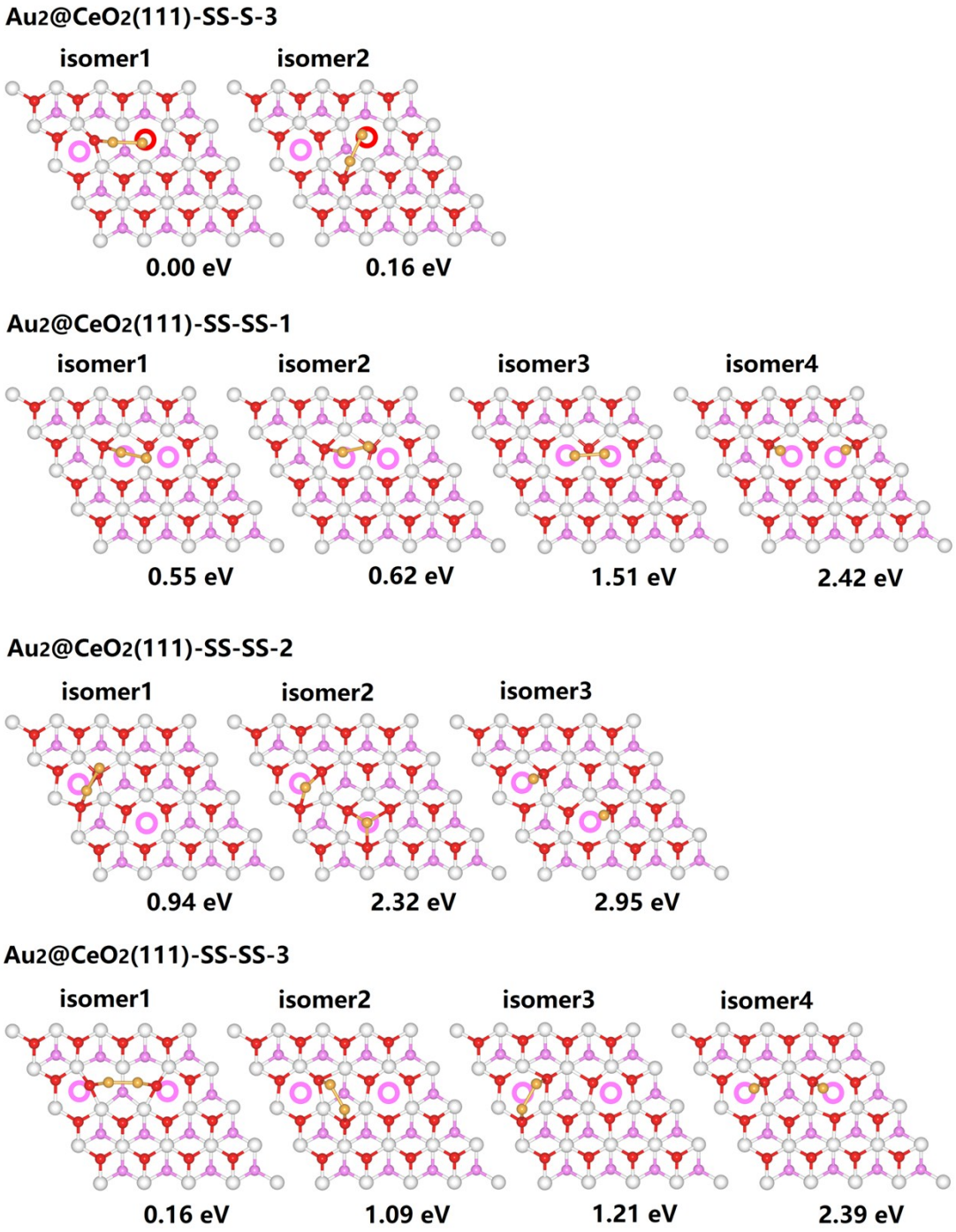

Figure S5. Structures of $Au_2@CeO_2(111)$-S(SS)-S(SS)-N (N=1, 2 and 3). Cerium, surface oxygen, and subsurface oxygen atoms are depicted in white, red, and pink, respectively. Open circles represent oxygen vacancies. For clarity, only the first O–Ce–O trilayer (TL) is shown. Energies are relative to the most stable structure.

Table S4. Multiple configurations of the excess 4*f* electrons on $Au_2@CeO_2$-SS-S-3, $Au_2@CeO_2$-S-S-1, and $Au_2@CeO_2$-SS-SS-3. Energies are relative to the most stable configuration. Calculated with p (4×6) periodicity, 3 CeO_2 trilayers and Γ-point. The configurations of the 4*f* electrons are corresponding to Figure S1.

Types	Configurations $\Delta^{E_v^a}$ (eV)						
	234-B	4-BCE	3-BCE	BCDE	1234	2-BE	23-B
	0.00	0.04	0.08	0.10	0.16	0.54	0.56
$Au_2@CeO_2$-	34-B	13-F	12-E	24-B	134	14-CE	123
SS-S-3	0.57	0.59	0.60	0.61	0.63	0.65	0.68
	1-DF	124					
	0.69	0.73					
$Au_2@CeO_2$-	4-B	14	34	AC	13	1-C	12
S-S-1	0.05	0.06	0.08	0.11	0.13	0.20	0.23
$Au_2@CeO_2$-	12-DF	14-BD	124-F	134-D	1-BDF	1234	ABCD
SS-SS-3	0.16	0.18	0.21	0.22	0.25	0.27	0.29

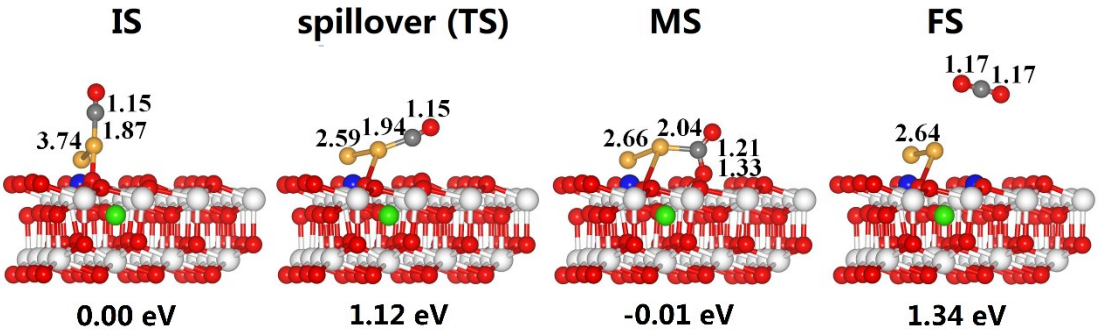

Figure S6. Calculated reaction path and corresponding energetics for the oxidation of CO catalyzed by $Au_2@CeO_2(111)$ via $O_{lattice}$ + CO_{ad} mechanism. Gold atom, cerium atom, oxygen atom, carbon atom, surface oxygen vacancy and subsurface oxygen vacancy are in gold, white, red, grey, blue and green, respectively.

References:

S1. J. P. Perdew, K. Burke and M. Ernzerhof, *Physical Review Letters*, 1996, **77**, 3865.

S2. G. Kresse and J. Furthmüller, *Physical Review B*, 1996, **54**, 11169.

S3. G. Kresse and J. Furthmüller, *Computational Materials Science*, 1996, **6**, 15-50.

S4. S. Dudarev, G. Botton, S. Savrasov, C. Humphreys and A. Sutton, *Physical Review B*, 1998, **57**, 157

S5. M. Nolan, S. C. Parker and G. W. Watson, *Surface Science*, 2005, **595**, 223-232.

S6. B. Meredig, A. Thompson, H. Hansen, C. Wolverton and A. Van de Walle, *Physical Review B*, 2010, **82**, 195128.

S7. J. Rabone and M. Krack, *Computational Materials Science*, 2013, **71**, 157-164

S8. M. V. Ganduglia-Pirovano, *Catalysis Today*, 2015, **253**, 20-32.

S9. P. E. Blöchl, *Physical Review B*, 1994, **50**, 17953.

S10. G. Henkelman, B. P. Uberuaga and H. Jónsson, *The Journal of Chemical Physics*, 2000, **113**, 9901-9904.